Pharmaceutical Research, Vol. 23, No. 10, October 2006 (© 2006)
DOI: 10.1007/s11095-006-9086-2

Research Paper

Analysis of Amorphous and Nanocrystalline Solids from Their X-Ray Diffraction Patterns

Simon Bates,[1] George Zografi,[2] David Engers,[3] Kenneth Morris,[3] Kieran Crowley,[4] and Ann Newman[1,5]

Received February 1, 2006; accepted May 31, 2006; published online September 22, 2006

Purpose. The purpose of this paper is to provide a physical description of the amorphous state for pharmaceutical materials and to investigate the pharmaceutical implications. Techniques to elucidate structural differences in pharmaceutical solids exhibiting characteristic X-ray amorphous powder patterns are also presented.
Materials and Methods. The X-ray amorphous powder diffraction patterns of microcrystalline cellulose, indomethacin, and piroxicam were measured with laboratory XRPD instrumentation. Analysis of the data were carried out using a combination of direct methods, such as pair distribution functions (PDF), and indirect material modeling techniques including Rietveld, total scattering, and amorphous packing.
Results. The observation of X-ray amorphous powder patterns may indicate the presence of amorphous, glassy or disordered nanocrystalline material in the sample. Rietveld modeling of microcrystalline cellulose (Avicel® PH102) indicates that it is predominantly disordered crystalline cellulose Form Iβ with some amorphous contribution. The average crystallite size of the disordered nanocrystalline cellulose was determined to be 10.9 nm. Total scattering modeling of ground samples of α, γ, and δ crystal forms of indomethacin in combination with analysis of the PDFs provided a quantitative picture of the local structure during various stages of grinding. For all three polymorphs, with increased grinding time, a two-phase system, consisting of amorphous and crystalline material, continually transformed to a completely random close packed (RCP) amorphous structure. The same pattern of transformation was detected for the Form I polymorph of piroxicam. However, grinding of Form II of piroxicam initially produced a disordered phase that maintained the local packing of Form II but over a very short nanometer length scale. The initial disordered phase is consistent with continuous random network (CRN) glass material. This initial disordered phase was maintained to a critical point when a transition to a completely amorphous RCP structure occurred.
Conclusions. Treating X-ray amorphous powder patterns with different solid-state models, ranging from disordered nanocrystalline to glassy and amorphous, resulted in the assignment of structures in each of the systems examined. The pharmaceutical implications with respect to the stability of the solid are discussed.

KEY WORDS: amorphous; CRN; disorder; disordered nanocrystalline; glass; pair distribution function (PDF); RCP; Rietveld; total scattering; X-ray powder diffraction (XRPD).

INTRODUCTION

Typically, the occurrence of a noncrystalline solid form can be determined by observing the loss of the distinct X-ray powder diffraction (XRPD) peaks characteristic of crystalline order, and the appearance of a general "halo" pattern. Such 'X-ray amorphous' material is generally characterized further by thermal analysis in a differential scanning calorimeter (DSC) where the appearance of a glass transition temperature, T_g, confirms the noncrystalline nature of the material (1). There are, however, a number of different noncrystalline phases that can give broad halos in the measured XRPD data, the most commonly observed of which are supercooled liquids and glasses (2).

At the present time the two primary theoretical models of glassy/amorphous materials that have been relatively successful in predicting material properties are the random close packed (RCP) and continuous random network (CRN) models. In the RCP model, molecules pack to minimize the local free energy and maximize local entropy without any consideration of three-dimensional (3D) tiling, i.e., no long-range translational, orientational, or conformational symmetry (3). The local molecular packing within an RCP model need not be related to any crystalline packing arrangement, as shown in Fig. 1a. The CRN model, originally proposed by

[1] SSCI, Inc, 3065 Kent Ave, West Lafayette, Indiana 47906, USA.
[2] University of Wisconsin, Madison, Wisconsin, USA.
[3] Industrial and Physical Pharmacy, Purdue University, West Lafayette, Indiana, USA.
[4] Cardinal Health, Somerset, New Jersey, USA.
[5] To whom correspondence should be addressed. (e-mail: anewman@ssci-inc.com)

ABBREVIATIONS: API, active pharmaceutical ingredient; CRN, continuous random network; NN, nearest neighbor; NNN, next nearest neighbor; NNNN, next next nearest neighbor; LRO, long-range order; MCC, microcrystalline cellulose; MRO, medium-range order; PDF, pair distribution function; RCP, random close packed; SRO, short-range order; XRPD, X-ray powder diffraction.

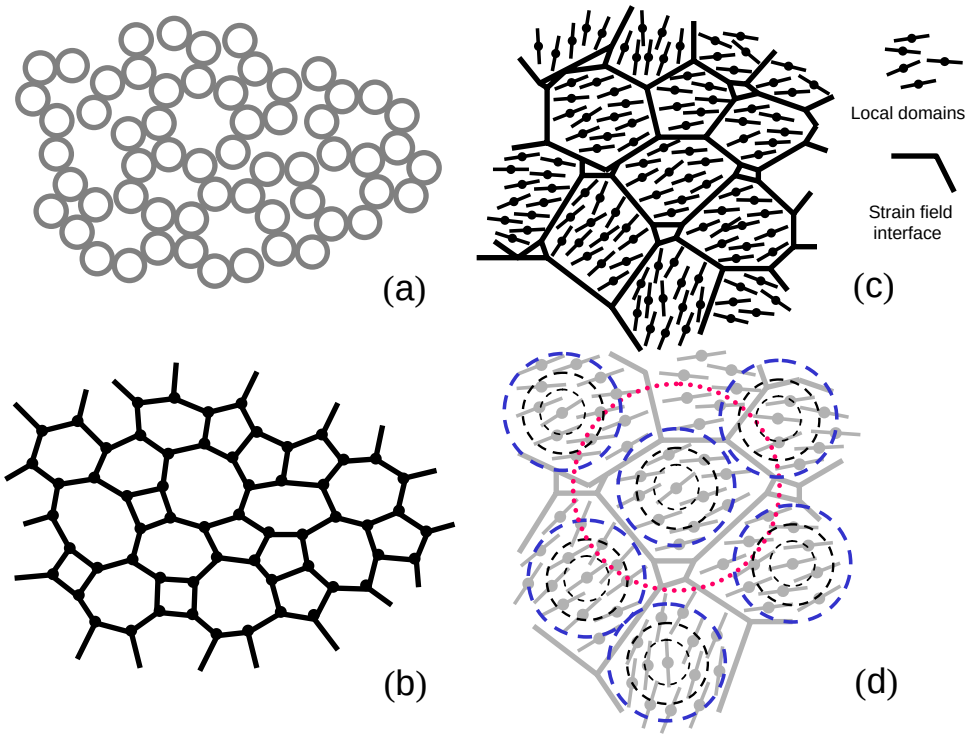

Fig. 1. Models of disordered phases; (a) random close packed, (b) continuous random network, (c) microstructural model illustrating the contribution of molecular anisotropy to local domain structure and strain field interface formation, and (d) enlargement of (c) illustrating the NN coordination observed using pair distribution functions.

Zachariasen (4), describes a glassy material that is characterized by a single optimum intermolecular bonding network. Typically, the preferred molecular packing will be representative of a 'high temperature' crystalline polymorph. Individual molecules will, however, exhibit a random distribution of bond angles and distances about the preferred packing arrangement. This is schematically represented in Fig. 1b. The relationship between the crystalline state and the glassy/amorphous state implied by these models can be further explored in terms of 'thermodynamic' and 'kinetic' disordering processes.

Three long-range order (LRO) symmetry operators (*translational, orientational, and conformational*) define the various solid forms available to an organic molecule. A crystalline system is defined by the presence of all three operators; the various mesophases (liquid crystals, condis crystals, and plastic crystals (5)) have one or two of the long range symmetry operators and the ideal amorphous state is defined by the absence of all three operators. Figure 2 outlines how the loss of these intrinsic LRO symmetry operators can lead to disordering of the crystalline phase resulting in various noncrystalline solid forms. The appearance of disorder in the solid state caused by the loss of the crystalline LRO operators is herein referred to as *thermodynamic* disordering due to the symmetry breaking nature of these transitions. Thermodynamic disordering allows for the appearance of random close packing in the amorphous state. In direct contrast to the discrete symmetry breaking thermodynamic disordering, Fig. 2 also outlines a more continuous disordering process where long-range order is reduced to short range order (SRO). The continuous process will be referred to as *kinetic* disordering and can occur for crystalline material or any of the mesophases. Kinetic disordering will, for example, reduce LRO crystalline material to SRO nanocrystalline material (6) or glassy material (7). Kinetic disordering preserves the local crystalline/mesophase packing symmetry into the glassy state. Thermal analysis of the liquid–solid transformation should exhibit a melt transition for any solid form defined by one or more order parameters (crystalline and mesophase) and a glass transition for a solid form defined by an absence of one or more order parameters (amorphous and mesophase).

A consideration of thermodynamic and kinetic disordering processes, as depicted in Fig. 2, suggest the existence of two different types of amorphous/glassy phases; the thermodynamic ideal amorphous and the kinetic glass. It is proposed that the ideal amorphous phase can be described by the RCP model and that the kinetic glass can be described by the CRN model. An ideal or true amorphous material is defined as isotropic, having no order (translational, orientational, or conformational) on any significant length scale (8). However, the complex molecular structures of pharmaceutical compounds automatically introduce local anisotropy to an amorphous system. To reflect this non-ideality, the term 'amorphous' or "RCP amorphous' is used in the context of this work to denote a material that has inherent SRO due to the local anisotropy present in the system but is isotropic on a macroscopic scale. For most organic molecular materials the SRO is not expected to extend over distances much larger than nearest neighbor (NN) or next nearest neighbor (NNN) interactions, which are typically less than 20–25 Å for small organic molecules (9). The CRN kinetic glass is inherently a metastable phase that will have different excess configurational entropy than the ideal amorphous because it retains

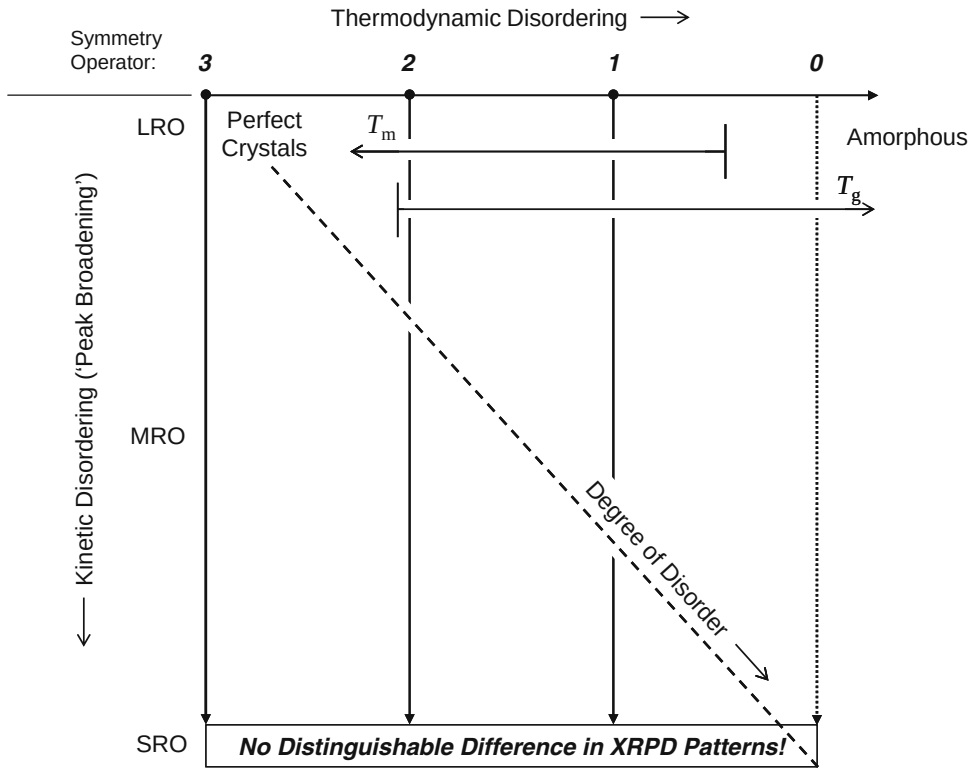

Fig. 2. Thermodynamic and kinetic disordering processes in solid systems illustrating the relationship between molecular order (translation, orientation, and conformation) and the length-scale of cooperativity; LRO, MRO and SRO. The *dashed line* reflects a projection of the 'degree of disorder' onto the kinetic–thermodynamic disordering plane, highlighting the similarity in the SRO and therefore the observed XRPD patterns, of different *solid phases*. In this view, a 'perfect crystal' is representative of a solid without any disorder and 'amorphous' reflects greatest degree of disorder. The ranges denoted for T_g and T_m represent systems that undergo a glass transition and melting, respectively.

the local molecular packing motif and bonding of the parent crystalline form (10).

An intermediate X-ray amorphous material within the *kinetic disordering* continuum is disordered nanocrystalline. Within the scope of this work, disordered nanocrystalline material refers to a solid form that retains the molecular packing motif of a parent crystalline polymorph but only over very short distances corresponding to a few nanometers. The actual order length scale will depend on the size of the molecule and the number of NN involved in the local order. This length scale is not the same as a particle size measured for powder samples. Glassy material like silica glass (7) is the end point of *kinetic disordering* within the solid state. In the glassy material, although the molecular packing motif will still be representative of a parent crystalline form, the concept of an average unit cell is no longer applicable. From X-ray diffraction measurements it is typically the length scale of the order that separates disordered nanocrystalline from glassy material. As such, X-ray diffraction measurements alone are often insufficient to distinguish the two phases. However, thermal analysis of a glassy phase should reveal a glass transition temperature, whereas only a melt would be expected for a nanocrystalline material.

Based on these concepts, the random nature of amorphous or glassy phases implies the existence of more densely packed regions (local domains) representing the average local order driven by the anisotropy of the molecule and less densely packed regions (microstructure) representing the interaction between the local domains. Our proposed amorphous model describing local domains of order surrounded by microstructure is shown schematically in Fig. 1c. Obtaining information about the order in the local domains using XRPD provides a better understanding of the amorphous material being generated.

Due to the complexity of noncrystalline materials, it is important to understand their physical properties, be able to distinguish the different types of materials, and understand the nature of the glassy state. Consequently, in depth analysis of the X-ray diffraction patterns is required, as well as additional measurements of structure to establish the true nature of X-ray amorphous materials. To this end, materials that have been rendered noncrystalline through cryogenic grinding have been analyzed by various methods and classified as disordered nanocrystalline, glassy, or amorphous materials. By examining the features of the pair distribution function (PDF) of material after different grinding times, it will be demonstrated that changes can be identified related to the crystalline form that arise from the stresses induced during grinding. XRPD and PDF data are discussed for microcrystalline cellulose (MCC), indomethacin (11), and piroxicam (12) materials. In conclusion, the pharmaceutical implications of observed differences in the type of X-ray amorphous material formed and its

stability will be discussed. This report is the first in a series of papers from our laboratories to discuss the characterization and understanding of amorphous and noncrystalline materials.

EXPERIMENTAL

Systems Analyzed

Microcrystalline cellulose (MCC), Avicel® PH102, was obtained from FMC Corporation (Philadelphia, PA). The sample was analyzed using a Bruker D-8 Discover diffractometer and Bruker's General Area Diffraction Detection System (GADDS, v. 4.1.20). An incident beam of Cu Kα radiation was produced using a fine-focus tube (40 kV, 40 mA), a Göbel mirror, and a 0.5 mm double-pinhole collimator. The sample was packed between 3-μm thick films to form a portable disc-shaped specimen. The prepared specimen was loaded in a holder secured to a translation stage and analyzed in transmission geometry. A beam-stop was used to minimize air scatter from the incident beam at low angles. Diffraction patterns were collected using a Hi-Star area detector located 15 cm from the sample and processed using GADDS. The intensity in the GADDS image of the diffraction pattern was integrated using a step size of 0.01° 2θ. The integrated patterns display diffraction intensity as a function of 2θ. Prior to the analysis a silicon standard was analyzed to verify the Si 111 peak position.

A sample of quench melt indomethacin was prepared for model development and was analyzed using a Shimadzu XRD-6000 X-ray powder diffractometer using Cu Kα radiation. The instrument is equipped with a long fine focus X-ray tube. The tube voltage and amperage were set to 40 kV and 40 mA, respectively. The divergence and scattering slits were set at 0.5° and the receiving slit was set at 0.15 mm. Diffracted radiation was detected by a NaI scintillation detector. A θ–2θ continuous scan at 3°/min (0.4 s/0.03° step) from 2.5 to 60°2θ was used. Five scans were collected per sample and the measured counts of each scan were added. A silicon standard was analyzed to check the instrument alignment. Data were collected and analyzed using XRD-6000 v. 4.1. Samples were prepared directly in an aluminum holder for analysis.

XRPD data previously reported for quench melt and cryoground indomethacin (11) and piroxicam (12) were further analyzed using the methods described below.

Materials and Methods

The measured X-ray powder patterns from disordered nanocrystalline/glassy and amorphous materials will all exhibit the broad halos characteristic of X-ray amorphous material. A visual inspection of the measured X-ray amorphous patterns and their relationship to the crystalline powder patterns can provide some suggestion as to the type of material that may be present. The diffuse halos present in X-ray amorphous patterns from disordered nanocrystalline material will show strong correlation to the diffraction peaks present in the powder pattern of the parent crystalline polymorph. The transition from disordered nanocrystalline to glassy may cause the position of the diffuse halos to move with respect to the diffraction peak from the parent crystalline form but the overall intensity envelope of the two powder patterns should be similar. The diffuse halos in the X-ray amorphous pattern for thermodynamic amorphous material may show no correlation to either peak positions or the intensity envelope observed in the powder pattern of the parent crystalline polymorph. Although some information can be extracted through analysis of the measured X-ray amorphous patterns, any direct analysis of the measured X-ray powder patterns without consideration of the underlying molecular packing can lead to ambiguous conclusions. The most self-consistent approach to the analysis of X-ray amorphous data is to start with an appropriate molecular packing model and work towards the X-ray diffraction pattern. This type of analysis requires a different set of analytical tools than those traditionally used to analyze X-ray powder data.

Pair Distribution Functions (PDF)

The PDF is a total diffraction approach to studying the structure of both amorphous and crystalline materials, providing a fingerprint of the inter-atomic distances that define a particular solid form (3). The PDF is presented as probability against distance and represents the weighted probability of finding two atoms separated by a distance r (13). The peaks in the PDF correspond to commonly occurring interatomic distances, where the product of peak area and distance gives the number of atoms involved weighted by the number of electrons per atom. A PDF trace is a robust one-dimensional representation of a radially averaged three-dimensional structure (14–18), as shown in Fig. 1d.

Following Warren (19) the PDF is simply the Fourier sine transform of the reduced structure factor representation of the measured XRPD data. The most critical step in deriving the PDF is the reduction of the measured data in 2θ to the reduced structure factor $S(Q)$. Then the data must be corrected for experimental aberrations including absorption, lorentz-Polarization, multiple scattering, instrumental background and thermal contributions (20,21). The corrected data expressed in terms of Q can then be reduced to remove the average electronic form factor giving $S(Q)$ in a form suitable for transformation into a PDF. The qualitative form of the reduced structure factor is used in ensuring a PDF trace free of artifacts induced by the Fourier transformation. The reduced structure factor should oscillate around zero moving continuously to the base line at both low and high Q. A further measure of the PDF 'quality' for quantitative analysis is that integration over the complete reduced structure factor gives the average material density (21). PDF analyses performed in this study used software developed internally based on published equations (19).

Most data published on the use of PDFs require the measurement of data on synchrotron systems out to large Q-values (22). However, the combination of atomic/molecular form factors and thermal vibrations present in molecular organic materials causes the measured X-ray intensity for intermolecular correlation to fall off to background levels between 40 or 60°2θ when using Cu Kα radiation (λ~1.5406 Å). This rapid intensity fall off means that data collected on standard laboratory powder diffraction systems is sufficient to calculate PDFs that capture the relevant intermolecular ordering information. The reduced measurement range does

however, reduce the spatial resolution of the resulting PDF. As with any Fourier transform-based analysis technique, the presence of significant noise levels within the measured XRPD data or false termination steps can lead to the appearance of spurious correlations within the PDF. This problem is especially serious, when analyzing X-ray amorphous materials (due to the low signal-to-noise) and can be minimized by averaging the results of multiple measurements and by collecting data and background at both high and low angles.

A direct comparison of experimentally determined PDF traces is a straight forward method for identifying possible kinetically disordered materials. For kinetically related materials, the same PDF peaks are to be expected at short distances. Once a kinetic disordered material has been identified, the challenge is to determine the disordering process that relates the PDF peak intensities and longer distance PDF peak positions. The breaking of 3D crystal symmetry that occurs with the thermodynamic transition into an amorphous phase typically causes the PDF peaks from the amorphous phase to move more significantly with respect to the PDF peaks from the crystalline phase. If the comparison between experimental PDF traces for an ordered and disordered phase show significant movement of the first inter molecular peak positions, this is an indicator that a thermodynamic transition has taken place and that the materials may not be kinetically related.

Rietveld Method

Although the Rietveld method was originally developed for single crystal structure solution (23,24), it has been extensively applied for quantitative analysis and microstructure analysis. The core of the Rietveld approach is a single crystal structural model of each phase being analyzed. In principle, the kinetic disordering of a crystalline material can be treated as a crystalline phase with variable microstructure (crystal size, micro-strain and defects) (25,26). The Rietveld analysis results presented here were derived using MAUD, v.1.998 (27).

However, the Rietveld method has a number of significant weaknesses when dealing with materials exhibiting SRO. Perhaps the most commonly reported problem is the use of discrete structure factors, which are only evaluated at the expected Bragg diffraction positions. For XRPD patterns with broad halos, the continuous variability of the material structure factor can cause peak shape and peak position changes that cannot be described using discrete structure factors (28). With the Rietveld method being based on coherent diffraction peaks it is also unable to model the incoherent diffuse X-ray which may be the dominant contribution for X-ray amorphous materials.

Total Scattering Method

To extend the original Rietveld method towards kinetically disordered materials, a new X-ray powder pattern simulation approach has been developed using a continuous structure factor extension to the original Rietveld approach that includes the possibility of single random defects and correlated pair random defects (29). The implementation of this method will be discussed in a forth coming paper (30). Using this total scattering model, X-ray diffraction from nanocrystalline/glassy and disordered crystalline materials is described by a combination of coherent and incoherent scattering profiles. Because of the random nature of the molecular arrangements in the glassy phases, however, the concept of a single average unit cell used in traditional powder pattern calculation is often not sufficient to describe the observed X-ray diffraction within the continuous structure factor model. For glassy materials, the continuous structure factor is evaluated over multiple unit cells with randomly displaced molecules in an attempt to model the random nature of the material. The use of an expanded unit cell also removes the dominating small angle scattering component calculated by the total scattering models based upon a single average unit cell. The molecular models used to derive the total scattering may also be used to derive simulated PDF's.

Amorphous Packing Model (APM)

Modeling the X-ray diffraction from the thermodynamic amorphous phase at the molecular level requires a different theoretical approach, as the molecular packing by definition is not related to any crystalline unit cell. The ideal approach would be to generate a randomly packed ensemble of molecules or molecular complexes using computer simulation techniques like Monte Carlo or molecular dynamics. However, to date, computational modeling has only been successfully applied to the random packing of ideal 'molecules' such as spheres, rods, ellipses and rectangles (31–33). If a random packing arrangement could be generated, then the pair distribution function of that arrangement can be used to generate the X-ray powder pattern (34), or can be directly matched to an experimentally derived PDF.

Simplified models of the expected molecular packing within the thermodynamic amorphous phase can be proposed based upon the emergent characteristic of randomly packed systems that molecules tend to form short range uniaxial stacks characterized by the shortest intermolecular packing distances. Using the KAP approach (35) and minimizing the local molecular free energy, it is relatively straight forward to generate possible molecular packing arrangements for the amorphous state. If a PDF transform of a measured X-ray amorphous pattern has been made, then the most likely packing distances along with their relative abundance can be determined in advance. This local nearest neighbor approach to modeling the thermodynamic amorphous material may return a number of different local molecular packing arrangements that give similar packing distances. To help identify the most appropriate local packing model, the X-ray powder pattern for the nearest neighbor arrangements can be simulated from the derived PDF or using a similar total scattering model as used for the glassy material (30).

The emergent property of short range uniaxial packing along the shortest intermolecular packing directions has a significant implication for measured X-ray powder patterns for amorphous materials. Depending on the degree of molecular anisotropy, there may be up to three preferred packing directions. Each preferred packing direction within an amorphous material will give rise to a diffuse diffraction halo in the measured powder pattern.

RESULTS AND DISCUSSION

The materials analyzed in the following section all appear to be X-ray amorphous in nature, exhibiting three or fewer primary diffraction halos in the measured X-ray powder patterns. The nature of the local molecular order, however, is proposed to be different for each material. The examples are focused on four broad categories of materials that can give rise to X-ray amorphous patterns (disordered nanocrystalline, glassy, amorphous, and mixed systems). Analysis of mesophases as an example of X-ray amorphous solids was determined to be outside the scope of this work.

Disordered Nanocrystalline Materials

Disordered nanocrystalline materials are solids that have lost their long-range crystalline order and have become disordered, but are not amorphous. The broad X-ray amorphous halos observed in disordered nanocrystalline materials are related to the crystalline microstructure (crystal size, micro-strain and defects) and are correlated to parent crystalline peaks.

In pharmaceutical systems, including drug substances, grinding crystalline material to produce disordered nanocrystalline material results in XRPD patterns where the peaks are observed to continuously broaden upon grinding due to loss of LRO. The observation of continuous peak broadening throughout the disordering process is indicative of the formation of disordered nanocrystalline material. For a disordered nanocrystalline system, there is a continuum of states between LRO and SRO, which are proposed to be a single thermodynamic phase with varying degrees of kinetic disorder.

Microcrystalline Cellulose

Microcrystalline cellulose is commonly treated as an amorphous material although there has been some uncertainty over the exact nature of the solid form. Indeed the key solid state characteristics, i.e., compaction properties, show that it undergoes significant plastic deformation consistent with a highly disordered solid. Due to its ubiquitous use in product development and lack of clarity around its structure, it provides a useful illustration of the methods under discussion. Cellulose exists in a number of different crystalline polymorphic forms that depend on the source of the material as well as the manufacturing process. Native cellulose (cellulose I), occurs as partially crystalline microfibrils composed of mixtures of two different crystalline polymorphs, cellulose Iα and Iβ. The ratio of these forms varies depending on the natural source and only recently have the forms been available in a sufficiently pure form for crystal structure analysis (36,37).

Microcrystalline cellulose is commonly used as a binder in pharmaceutical formulations where it is frequently referred to as being an amorphous excipient. The dry T_g of microcrystalline cellulose is reported as 221 (38) and 235°C (39). A recent report (40) of crystalline cellulose has demonstrated the utility of Rietveld modeling for investigating disordered nanocrystalline material in microcrystalline cellulose samples from a variety of sources. Depending on the correlation length within the crystalline regions (crystal size), traditional Rietveld methods may be able to accurately model the broadening of the coherent diffraction peaks. However, the Rietveld method will be unable to directly model the appearance of any incoherent diffuse (X-ray amorphous) scattering.

As suggested by its name, microcrystalline cellulose should represent an ideal material to demonstrate X-ray amorphous patterns driven by nanocrystalline disorder. The data in Fig. 3 represents an XRPD measurement of microcrystalline cellulose (Avicel® PH102). Using the published crystal structures for Forms Iα, Iβ and II of cellulose (36,37,41), traditional Rietveld modeling determined that the MCC sample contained no significant amounts of cellulose forms Iα and II, but did contain Form Iβ. The average crystal size used to achieve the best fit was 10.9 nm, establishing it as disordered nanocrystalline. However, the shape of the residual from the Rietveld modeling indicated that a significant diffuse X-ray amorphous component was present. Within the traditional Rietveld approach the diffuse X-ray amorphous scattering can be treated as one or more broad peaks. The best fit to both the residual and the original measured data suggested a single halo X-ray amorphous contribution centered at 21.4°2θ. Taking the ratio of the total diffuse X-ray intensity to the total nanocrystalline X-ray intensity gave an estimated concentration of approximately 26 wt.% X-ray amorphous. The concentration returned by a single sample Rietveld analysis cannot be considered to be a true quantitative number, however, this value is consistent with a previously published value of 37 wt. % (42). The microstructure of MCC is known to be variable so it is not unexpected that the percentage amorphous values differ slightly. The disordered nanocrystalline and X-ray amorphous components are displayed in Fig. 3 along with the best fit and measured XRPD data. The Rietveld analysis readily confirms the presence of both disordered nanocrystalline Form Iβ and X-ray amorphous cellulose, However, the traditional Rietveld approach gives little reliable information concerning the molecular level structure present in the X-ray amorphous phase.

Amorphous Materials

Within this study, the thermodynamic amorphous phase has been defined with respect to the crystalline polymorphs. As such, cryo-grinding studies provide an ideal experimental approach to investigate the formation of amorphous material and the nature of the X-ray diffraction response. The typical behavior observed when grinding a crystalline organic material to produce amorphous material is that an increasing percentage of the crystalline material will collapse to amorphous as a function of grinding time. The amorphous local packing generates broad halos in the XRPD pattern that are not correlated to the crystalline peaks. If no significant change is observed in the crystalline diffraction peaks upon grinding, the ground sample can be modeled as a phase separated binary mixture of thermodynamic amorphous and crystalline materials. For clarity, this type of relationship between crystalline and amorphous phases will referred to as Type I (Fig. 4).

Indomethacin

An example of a material exhibiting Type I amorphous behavior is indomethacin. Three unsolvated forms of indo-

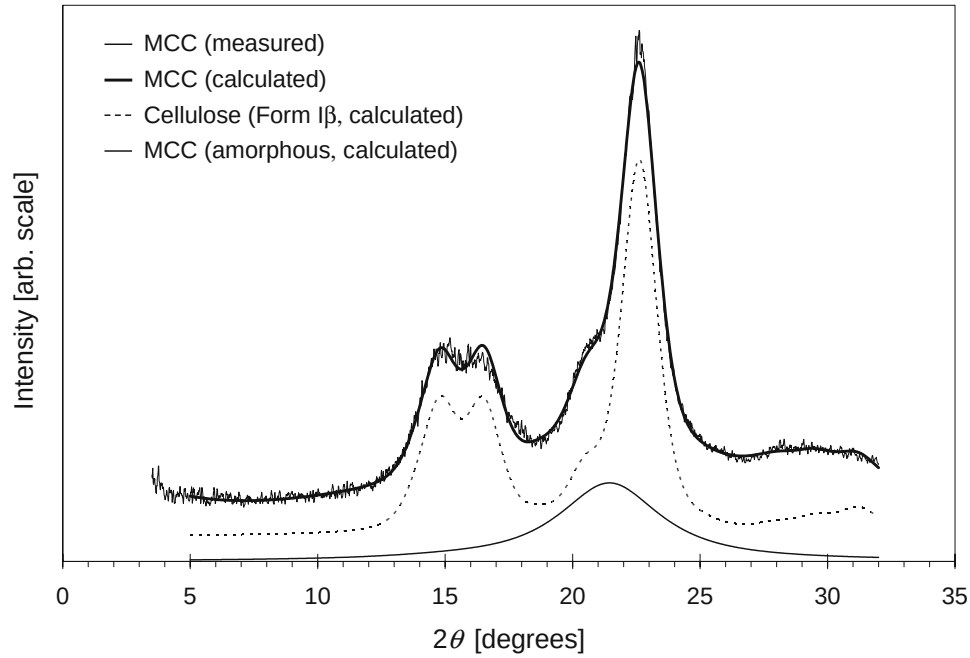

Fig. 3. Rietveld modeling studies of microcrystalline cellulose showing the measured and calculated XRPD patterns for Avicel® PH102 (*overlaid*). The calculated pattern was composed of disordered nanocrystalline Form Iβ (*middle*) and a single dominant X-ray amorphous halo (*bottom*) at about 21.4°2θ. The shape and position of the X-ray amorphous halo was determined from the residuals of the initial Rietveld refinement using only crystalline Form Iβ cellulose. The shape and position of the inferred X-ray amorphous peak is consistent with amorphous cellulose and corresponds to approximately 26 wt.%.

methacin (α, γ and δ) are known, and grinding studies of these forms have been performed (11). XRPD data obtained from these grinding studies are further analyzed here.

As shown in Fig. 5, cryoground γ indomethacin exhibits no peak broadening, indicating a phase separated binary mixture. Sixty minutes of cryogrinding produces an amorphous material. The same trend is observed for cryoground ground α and δ indomethacin samples. After grinding, the amorphous patterns produced from the three forms are essentially the same, as shown in Fig. 6. The amorphous pattern of the quench melt material has been added for comparison and it is evident that the same amorphous halo is obtained. These data indicate that a common X-ray amorphous form is produced for indomethacin.

To obtain more information from the XRPD data, PDFs were calculated. The PDFs of all ground indomethacin samples show the loss of LRO with continued grinding. After 30 min of grinding, interactions greater than approx-

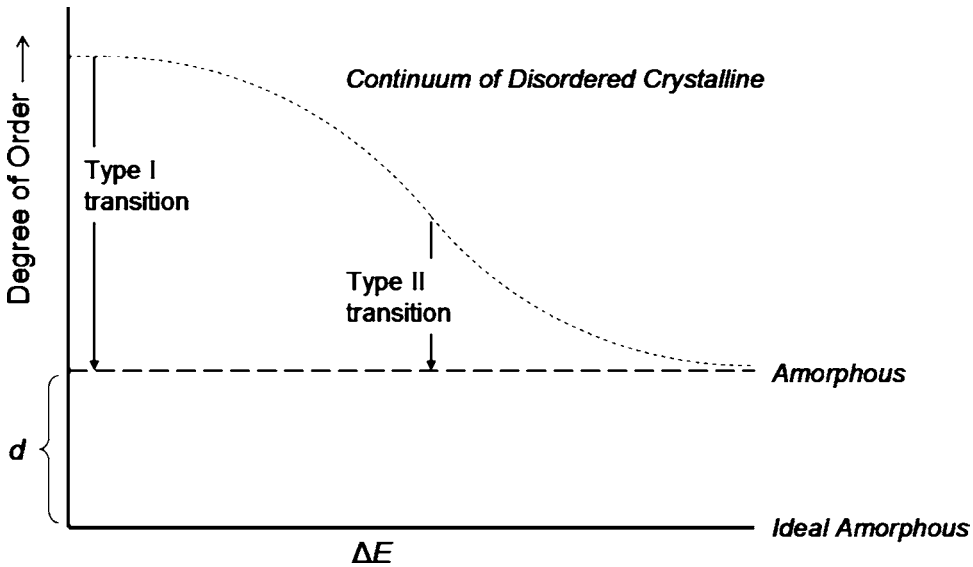

Fig. 4. Schematic of the disordering of crystalline solids. The distance d reflects the increase in local structural order relative to an ideal amorphous material and is a manifestation of the increase in cooperativity due to anisotropy.

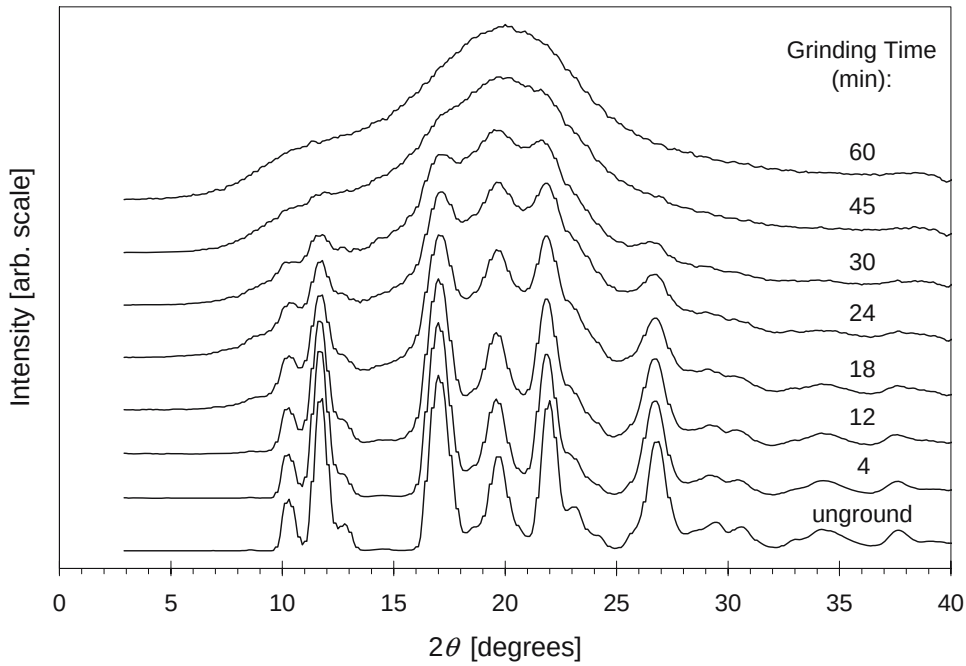

Fig. 5. XRPD patterns of unground and ground γ indomethacin (*bottom to top*); 4, 12, 18, 24, 30, 45, and 60 min of grinding. Note: no significant change in peak width is observed with increased grinding time.

imately 40 Å are not readily observed, but NN and NNN interactions (SRO) are still intact in these samples (data not shown). The PDFs of the ground (60 min) and melt quench indomethacin samples are also similar when compared. The PDF of the melt quench material is given in Fig. 7 shows that the NN and NNN peaks corresponding to the molecular coordination spheres are clearly visible. The dominant PDF peak (NN) corresponds to a molecular packing distance of approximately 4.6 to 4.7 Å. With the inclusion of van der Waals radii, the peak at 4.7 Å corresponds to the indomethacin molecular thickness. This axis is expected to be the primary packing axis because it is the shortest molecular axis and it is normal to the molecular plane. A weaker lower angle halo in the X-ray amorphous pattern corresponds to a packing distance of approximately 9.2 Å, driven by the intermediate length molecular axis. The appearance of the two shortest molecular dimension in the measured XRPD pattern is a strong indicator that the indomethacin forms are thermodynamic amorphous material from a Type I transformation.

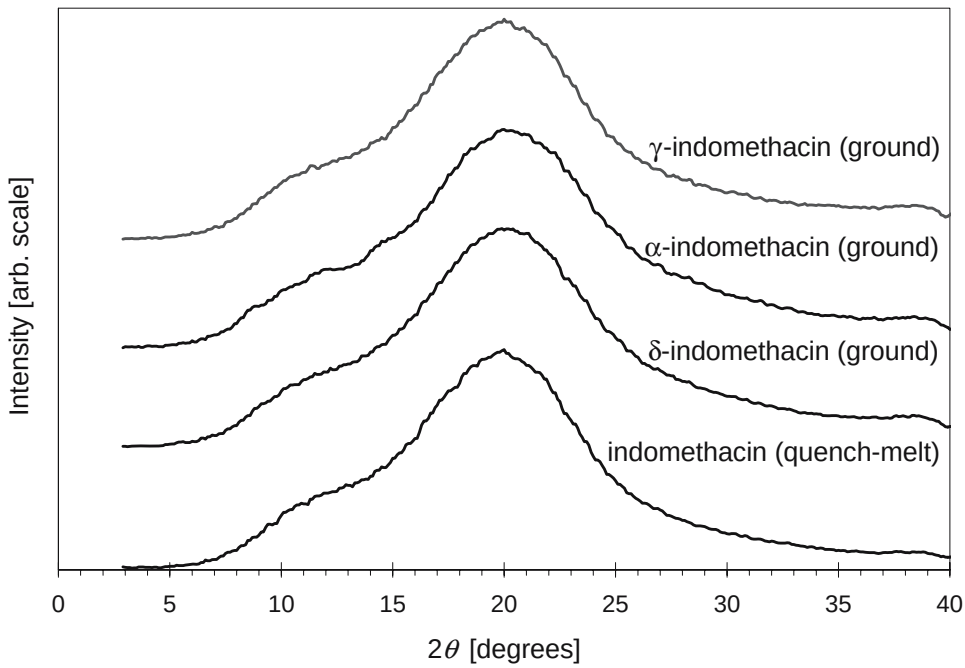

Fig. 6. XRPD patterns of amorphous indomethacin samples, (*top to bottom*): ground δ, ground α, ground γ, and quench melt. The same X-ray amorphous pattern is observed for all samples.

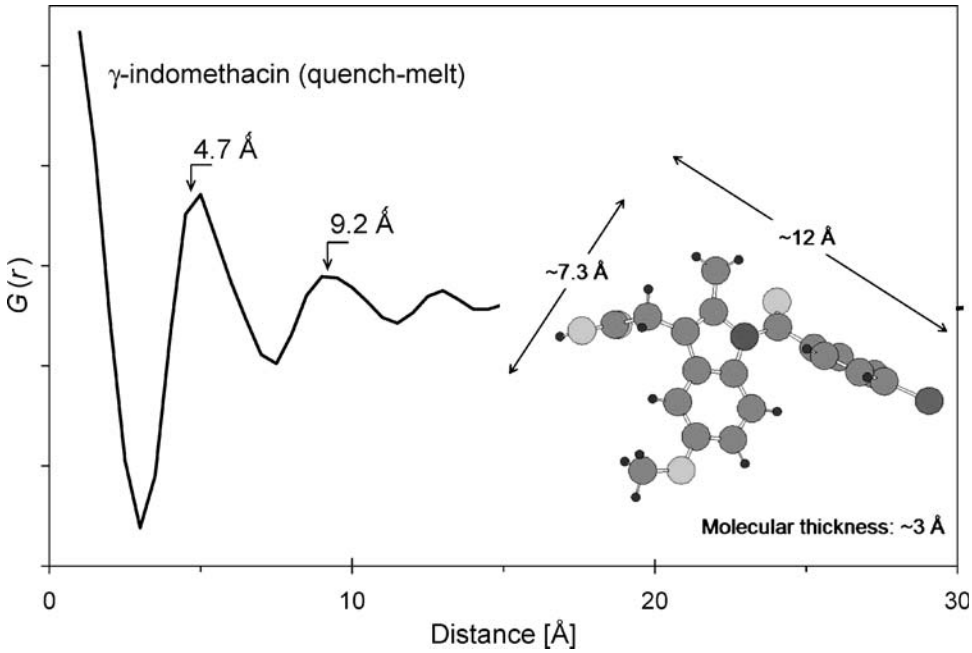

Fig. 7. PDF of quench-cooled melt preparation of γ indomethacin with a NN and NNN peak position of 4.7 and 9.2 Å, respectively.

Repeating the analysis performed on MCC using the traditional Rietveld method, the crystallite size for the three known crystalline polymorphs (γ, α, δ) was decreased below 60 Å to calculate patterns representing disordered nanocrystalline data. None of the individual crystalline polymorphs were able to provide a good fit to the measured X-ray amorphous data. Figure 8 (line a) shows the 'best' fit achieved using the γ crystalline form with the following isotropic microstructural parameters: crystal size ~60 Å, micro-strain ~11% and isotropic thermal parameter 8.5. The isotropic thermal parameter is used to model random molecular deviation within the average crystal structure.

A powder pattern generated using the total scattering model for γ indomethacin assuming a glassy structure is compared to both the experimental X-ray amorphous XRPD and the results of Rietveld modeling in Fig. 8. Neither of the

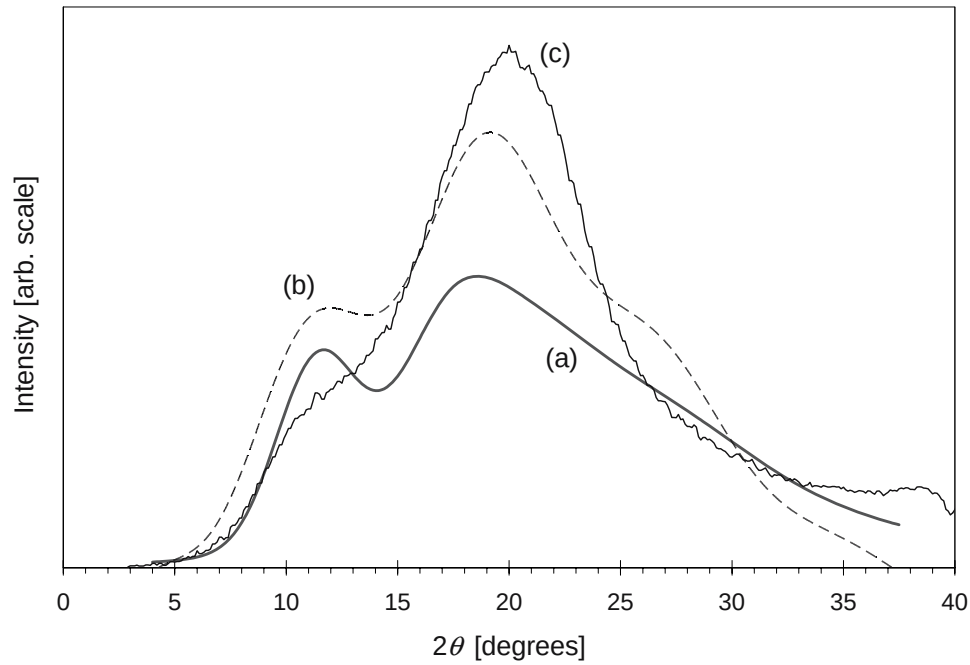

Fig. 8. Results of Rietveld (a) and total scattering (b) analysis of the X-ray amorphous XRPD pattern for indomethacin (c). Although the continuous structure factor in the total structure model is better able to describe the primary *halo shape and position*, neither model is able to reproduce the measured data. Being based upon the concept of an average crystal model, both calculated X-ray amorphous patterns exhibit too much structure.

simulated X-ray powder patterns based upon a γ indomethacin unit cell accurately describe the observed X-ray amorphous pattern. The simulated powder patterns exhibit either a broader halo or more structure than is visible in the measured X-ray amorphous pattern. Perhaps more importantly, the position of the primary halo is visibly shifted between the simulated and measured patterns, indicating a change in the local molecular packing arrangement. The simplicity of the measured X-ray amorphous data with respect to the simulated disordered nanocrystalline/glass data and the observed peak shift support the proposal that any 3D molecular correlations within an average unit cell have collapsed and that indomethacin forms a randomly packed thermodynamic amorphous phase.

The amorphous packing model was used to generate possible XRPD patterns from those local clusters that gave the lowest free energy and highest density. Figure 9 shows a comparison between the measured X-ray amorphous pattern and a simulated pattern from one of the possible local molecular clusters without any attempt to fit the data except for scaling. The simulated pattern is in good agreement with the measured pattern. The molecular arrangement used to generate the simulated powder pattern was derived from an RCP model, further supporting the validity of a thermodynamic amorphous indomethacin phase. These results indicate that the single common X-ray amorphous pattern observed for ground and melt/quench indomethacin is a product of a thermodynamic amorphous phase described by random close packing of the indomethacin molecule. Initial modeling indicates that the most favorable nearest neighbor molecular packing direction is normal to the plane of the molecule containing the indole ring and phenyl ring, similar to packing observed in the γ crystalline form (43). This NN arrangement is the shortest packing distance favored by the RCP model and also preserves the hydrogen bond dimer, as shown in Fig. 10. This finding is important in assessing and understanding the physical stability of the amorphous material, which will be discussed in a later section.

Supporting evidence for the indomethacin packing model generated by the RCP simulations comes from Raman and infrared measurements (44) which suggest that the majority of the indomethacin molecules in the amorphous state form hydrogen bonded cyclic dimers similar to the 'gamma' crystalline polymorph. Solid state NMR measurements on amorphous indomethacin using spin-lattice relaxation times to estimate molecular mobility show that 73% of the carbons were in a state of monodispersive relaxation (45). This suggests that the amorphous state is relatively homogeneous and restricted. The carbons in the molecular plane indole and phenyl rings showed slower mobility than the chain carbons which is consistent with the proposed RCP packing model. The molecular NN packing distances determined by the PDF indicate that a single molecule is the packing synthon in the amorphous phase. Although the resulting preferred packing allows the formation of a hydrogen bond dimer, the dominant number of dimers observed in the amorphous state indicates that the hydrogen bonding must be influencing the preferred local packing.

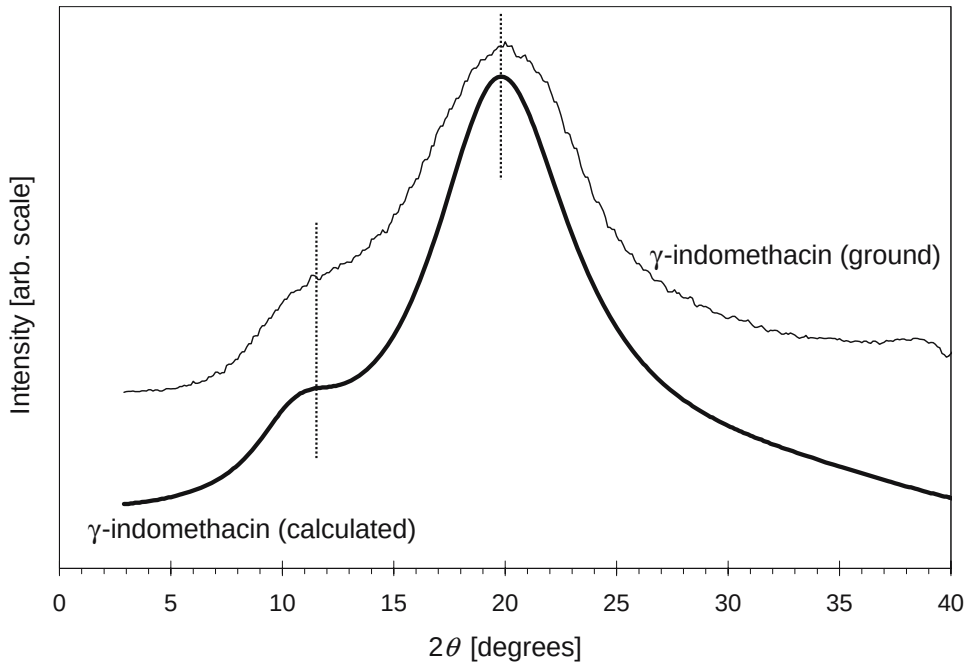

Fig. 9. Measured γ indomethacin X-ray amorphous pattern (*top*) and best fit simulated XRPD pattern using the amorphous packing model (*bottom*). The primary halo at ~20°2θ corresponds to an NN molecular coordination distance of approximately 4.7 Å, while the weaker second halo centered at about 11.7°2θ corresponds to a second NN coordination distance of approximately 8.7 Å. These packing distances do not correspond to the Bragg *d*-values for the measured peak positions due to the spherical averaging. The packing distances closely correspond to the two smallest molecular dimensions plus 1.5 Å. Note the 9.5 Å peak denoted on the PDF in Fig. 7 is related to the second harmonic of the primary NN packing distance and not the secondary packing direction revealed in the molecular packing study.

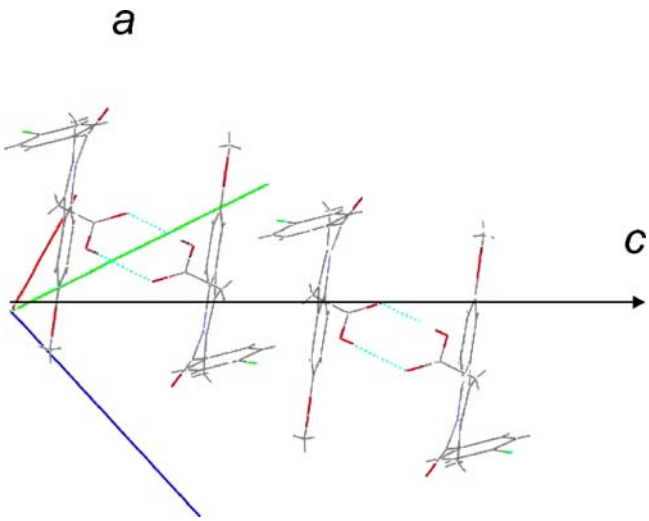

Fig. 10. Optimum NN molecular packing as derived from the amorphous packing model applied to the measured X-ray amorphous data of indomethacin. Note the primary packing direction occurs approximately normal to the molecular plane defined by the rigid 5 member and 6 member rings, allowing the formation of dimers similar to the published γ crystal structure.

The lack of broadening observed for the crystalline diffraction peaks upon grinding indicate that RCP amorphous indomethacin materials are produced from the known crystalline forms via a first-order-like Type I transformation.

Combined Glassy/Amorphous System

In contrast to the binary phase relationship observed for the Type I crystalline to amorphous transition, X-ray diffraction measurements of cryoground piroxicam (12) indicate that a more complex relationship between crystalline and amorphous forms is possible. Piroxicam is known to exist as two unsolvated forms, designated Forms I and II (12). The X-ray diffraction measurements of the cryogrinding study performed on the two polymorphs will be summarized and further analyzed in this section.

Piroxicam

The XRPD data collected during the cryogrinding of Form I indicated that Form I piroxicam behaved much like indomethacin. There was no observable diffraction peak broadening while the X-ray amorphous component was observed to increase with grinding time. The published Rietveld modeling of the X-ray amorphous pattern was unable to achieve a good fit, which was taken as an indication that the cryogrinding had produced a thermodynamic RCP amorphous phase. Form II was also found to go amorphous upon grinding; however, it revealed an intermediate X-ray amorphous contribution that was markedly different from the X-ray amorphous contribution observed on grinding the more stable polymorph, Form I. With continued cryogrinding of Form II, the intermediate X-ray amorphous contribution collapsed to an XRPD pattern that matched the X-ray amorphous pattern produced from Form I.

The intermediate Form II X-ray amorphous pattern closely followed the intensity envelope observed for the crystalline Form II XRPD pattern. Traditional Rietveld modeling of the intermediate X-ray amorphous contribution is able to achieve a reasonable fit with an effective crystal size of 1 nm, Fig. 11a. The high temperature piroxicam Form II crystal structure has a *b* lattice parameter of approximately 1.2 nm, so the effective crystal size from the Rietveld modeling is smaller than the crystal unit cell. With the same small crystal size, the fit to the measured intermediate X-ray amorphous data was very poor using coherent scattering from the total scattering model due to the dominant small angle scattering generated by such small crystalline units. The nonphysical crystal size along with the lack of agreement with the total scattering model suggest that modeling the intermediate X-ray amorphous phase as disordered nanocrystalline is not appropriate.

Neutron diffraction measurements on silica glass suggest that it is the incoherent scattering from the high temperature crystalline polymorph that provides the best description of the diffuse scattering in the glassy phase (7). Figure 11b shows a comparison between the measured intermediate X-ray amorphous pattern and the calculated incoherent scattering using the total scattering model. Without refinement of the piroxicam Form II crystal structure, the agreement between the calculated incoherent scattering and measured X-ray amorphous contribution is reasonably close. Although the agreement to the measured data is not as good as that achieved by the Rietveld refinement, modeling the disordered phase as a CRN glass is a better physical representation than a disordered nanocrystalline material with 1 nm effective crystal size. The observation of a glass transition for the intermediate X-ray amorphous form would confirm it as being a glass rather than a disordered nanocrystal.

It is proposed that cryogrinding of Form II piroxicam caused the LRO crystalline material to initially collapse towards a disordered nanocrystalline/glassy phase before finally transforming through a solid-state disorder to disorder phase transformation into an amorphous form. For clarity, this type of relationship between the crystalline and amorphous phase will be referred to as Type II (Fig. 4). The expected continuous diffraction peak broadening prior to the formation of a disordered nanocrystalline phase was not observed in the published data. This may be a result of expected rapid "recrystallization" or annealing of the partially disordered crystalline material before the XRPD data could be collected. The persistence of the crystalline Form II diffraction peaks with no observed peak broadening under cryogrinding may also result from a discrete collapse of the crystalline Form II structure into the glassy Form II piroxicam phase.

The more stable piroxicam Form I crystalline polymorph is known to form hydrogen bonded dimers in the solid state (12), similar to indomethacin. This is in contrast to the Form II crystalline polymorph that forms continuous hydrogen bond chains. The hydrogen bond chains may provide sufficient stabilization of the crystalline molecular packing allowing the crystalline Form II piroxicam to initially transform into a glass phase before becoming amorphous.

The PDF of ground piroxicam Forms I and II showed the loss of LRO with continued grinding with both forms collapsing into the final thermodynamic RCP amorphous phase. In the thermodynamic amorphous phase a reproducible local structure exhibiting three distinct NN order length

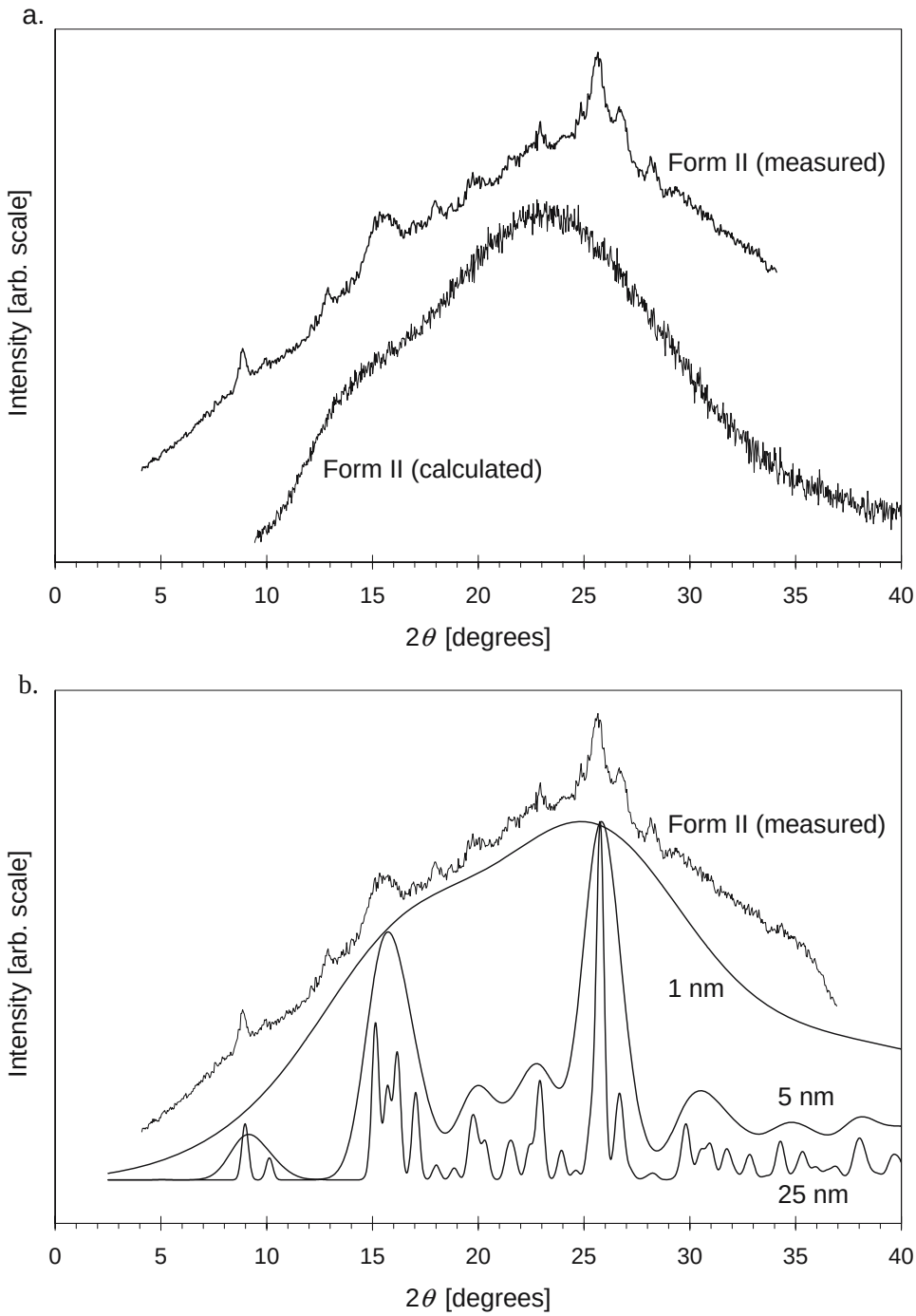

Fig. 11. (a) Measured amorphous XRPD pattern for cryoground piroxicam Form II (*top*) and simulated incoherent XRPD pattern (*bottom*) obtained using the total scattering model and a high temperature modification of the single crystal structure (ref ID: KAFYAR) from Cambridge Structural Database (*CCDC*). (b) Measured amorphous XRPD pattern for cryoground piroxicam Form II and Rietveld calculated XRPD patterns from nanocrystalline material with crystal sizes of 1, 5, and 25 nm. A high temperature modification of the single crystal structure (ref ID: KAFYAR) from Cambridge Structural Database (*CCDC*) was used for the Rietveld calculations.

scales at 4.8, 7.9, and 12.1 Å was observed (12). These characteristic peak positions corresponded to the dominant atom–atom distances in the amorphous phase and can be related to the molecular dimensions of the molecule. With the inclusion of van der Waals radii, the peak at 4.8 Å is approximately the molecular thickness, the peak at 7.9 Å approximates the molecular width, and the peak at 12.1 is approximately the molecular length. The amorphous form of piroxicam is unusual in that three uniaxial inter-molecular packing relationships are established rather than the expected and more common one or two. With the observed packing distances being related to the physical size of a single

molecule, the basic packing synthon in the amorphous state corresponds to a single molecule and not a dimer. However, analysis of the mechanochromism observed on the cryogrinding of both Form I and Form II into the amorphous state (46) indicate that only a small percentage of the hydrogen bonds are broken by the cryogrinding. Work is continuing in our lab to better understand the piroxicam system.

It is important to note that X-ray amorphous patterns obtained for ground piroxicam represented three types of materials: 1) RCP amorphous material obtained by a Type I transformation (Form I grinding), 2) disordered nanocrystalline/ CRN glassy material (Form II grinding), and 3) RCP amorphous material obtained by a Type II transformation (Form II grinding). Although the XRPD patterns of the amorphous forms derived from Type I or Type II transformations are almost indistinguishable, the stability of the materials was found to be different, as discussed in the next section.

Pharmaceutical Implications

A property of amorphous materials not explored so far that has direct consequences on the results that might be returned by different analytical techniques is the existence of microstructure. The formation of local short range order that minimizes the local free energy suggests the existence of local domains. The local molecular order is typically not crystalline in nature and therefore is not able to grow into long range order. This implies that it is the number of local domains that characterize amorphous materials and not necessarily the size of the domains. Due to the random nature of the amorphous phase, the relative high density local domains must be balanced by relative low density (high free energy) regions that form the microstructure. This is schematically depicted in Fig. 1c. Annealing of amorphous material is proposed to allow more of the initial microstructure to convert to the preferred local order. With a single thermodynamic amorphous phase, the average short range order within the local domains will be stable and reproducible from batch to batch. In contrast, the number of local domains and extent of the microstructure will strongly depend on how the amorphous material was formed and will directly influence a number of material properties such as stability. Whereas XRPD is more sensitive to the average local amorphous order in the local domains, other experimental probes such as enthalpy, volumetric relaxation, or water vapor absorption, are likely to reflect to some extent the properties of the microstructure. Characterization of amorphous/glassy systems, therefore, requires the use of complementary experimental probes which is currently being investigated in our laboratories.

Structural Aspects

As the above examples illustrate, obtaining a material that exhibits an amorphous halo can represent any number of "X-ray amorphous" or disordered phases, ranging from disordered nanocrystalline to amorphous. Even amorphous materials can differ based on the residual LRO present in the sample.

When developing an amorphous material, it is important to understand the type of disordered material being produced. As demonstrated with piroxicam, the amorphous material obtained can be dependent on the starting material and the process used to render it X-ray amorphous. This is one reason that amorphous materials produced from different crystalline forms or using different processes (milling, lyophilization, quench melt) can result in varying physical properties.

There are a number of ways to determine the type of disordered system. One method uses the peak broadening observed for the crystalline peaks in the XRPD pattern if partially amorphous material is available (such as from grinding the crystalline material or partial recrystallization from an amorphous solid). Samples that exhibit continuous peak broadening represent disordered nanocrystalline material. Samples that do not exhibit continuous peak broadening are amorphous materials. However, as observed with piroxicam, partially disordered nanocrystalline material is unstable to LRO and may transform before the peak broadening can be observed. Another method is examination of the PDF data. If the intermolecular peaks in the PDF of the X-ray amorphous material matches the initial crystalline material but exhibits a decay in peak height, the material is disordered nanocrystalline or glassy. Significant differences in the PDF traces between the two materials will indicate an amorphous material. Additional information can be obtained from the PDF analysis, such as the correlation length of NN and NNN interactions, which can help distinguish disordered nanocrystalline from a glass. A third way is to model the XRPD data. If a good fit is obtained for the experimental amorphous halo by decreasing the crystallite size in a Rietveld model, the material is potentially disordered nanocrystalline, provided the effective crystal size is physically realistic. If the parent crystalline unit cell within the total scattering model is able to describe the experimental data using the incoherent scattering contribution, then the material is most likely glassy. If an amorphous packing model readily fits the experimental data, the material can be considered to be amorphous.

From a practical standpoint, the type of disordered material obtained will also influence quantitation of partially amorphous samples. It is important to note that since disordered nanocrystalline materials form one continuous phase with crystalline material, quantitating the amount of "amorphous" material using crystalline/amorphous binary mixtures as standards is not applicable and will not result in representative values for the disordered material in the sample. Rietveld or total scattering modeling to determine material parameters, such as crystallite size and strain, is a more appropriate method to characterize these materials. For amorphous materials, the partially crystallized sample consists of two phases, therefore, quantitating the amount of amorphous material using binary phase mixtures of standards, as is often done for pharmaceutical systems (47), is appropriate.

Physical Stability

The development of the amorphous form of an active pharmaceutical ingredient (API) for use in solid dosage forms is desirable when the crystalline form does not provide the requisite pharmaceutical properties, particularly inade-

quate oral bioavailability due to poor aqueous dissolution, and when other approaches such as salt formation fail to solve the problem. Since amorphous solids are in a higher free energy state than the crystalline state, the development of amorphous API represents a significant risk whereby the compound might undergo re-crystallization over the time course of processing, storage and use of the product. Although some approaches are available to reduce crystallization rates, e.g., the use of solid dispersions of API and polymers (48), it is important to understand and characterize the intrinsic tendencies of amorphous API to crystallize under various conditions. It is well recognized that the crystallization of API from the amorphous state depends on structural, thermodynamic and kinetic factors (49). Of critical importance is the structure of the amorphous form at various temperatures and relative humidities, since this impacts strongly on the thermodynamic driving force for nucleation and on the molecular mobility of the system, as reflected in the relaxation times (50).

As shown in this study, the ground indomethacin materials exhibit broad halos in the XRPD pattern uncorrelated to the crystalline peaks, indicating a first-order-like Type I transition. Amorphous material produced via a first-order-like Type I transition may retain some residual memory of the initial crystalline phase due to the phase coexistence implied by a first-order transition. This 'memory' is observed for indomethacin where, upon crystallization, ground γ indomethacin converts back to crystalline γ indomethacin. A careful examination of the PDF for γ indomethacin amorphous material reveals features at larger intermolecular distances that are not a product of experimental error or truncation errors introduced by the PDF calculation. These weak features are seen to correspond to peaks in the PDF for crystalline γ indomethacin, Fig. 12. This is strong evidence that the amorphous material produced by cryogrinding γ indomethacin retains residual γ crystalline form. This residual LRO for the γ crystalline form can be considered a "memory effect" or possible "seeding effect" that has been postulated for a number of systems. The PDF provides evidence that LRO in amorphous materials can direct the crystal form produced under stress conditions. The PDF data for cryoground α indomethacin also helps explain the observed crystallization for this material (Fig. 13). The PDF for ground α indomethacin shows residual α indomethacin LRO, as well as additional structure, which is correlated to γ character (while it is not clear how the γ appears, it is known that below T_g, γ is the dominant phase and may form spontaneously (51)). Under stress, cryoground α indomethacin recrystallizes to γ and α indomethacin (11).

This is consistent with the observation that while grinding of the γ form led to the γ form upon recrystallization at 30°C, grinding of the α crystal form for 60 min resulted in mixture of α and γ forms upon recrystallization at 30°C (52). Further studies showed that a rapidly cooled quench melt, subsequently cryoground in liquid nitrogen for 60 min, produced an amorphous material with essentially the same T_g as a sample cryoground from the γ crystal for 60 min and the same specific surface area (11). However, isothermal crystallization from the quench cooled material at 30°C revealed that the rate of crystallization for the ground crystals was about five times greater than that observed for the ground quench melt. Such behavior would be consistent with the conclusion, presented above, that the formation of amorphous materials by cryogrinding of the α and γ crystal forms of indomethacin produces amorphous material with seeds of the original crystal form used.

Cryoground piroxicam provides a useful example of crystalline forms that convert upon grinding to amorphous material both spontaneously and through an intermediate short-range ordered phase. The XRPD pattern of piroxicam

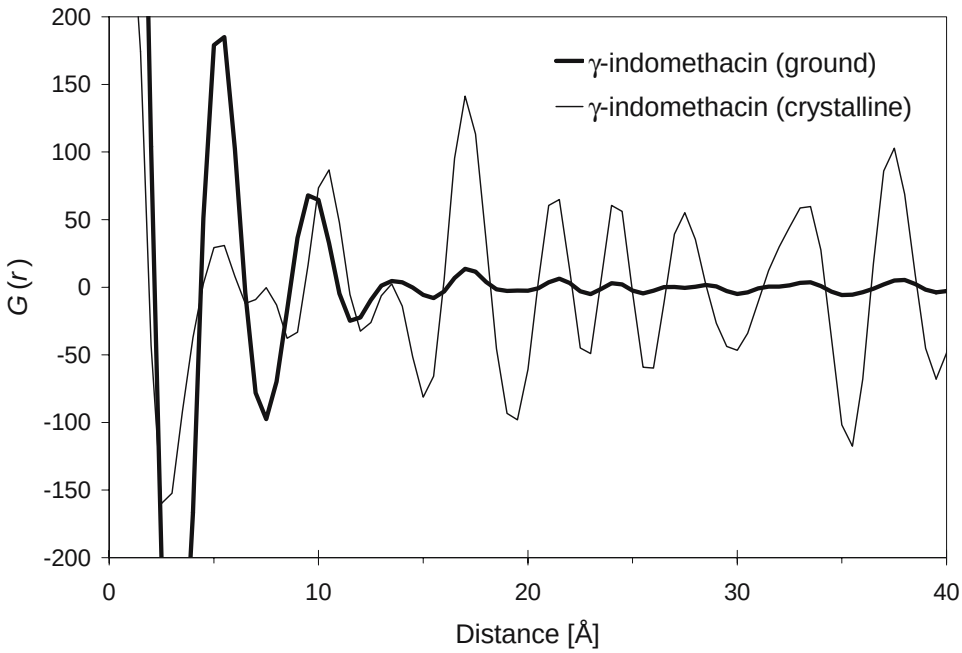

Fig. 12. PDF of ground γ indomethacin and crystalline γ indomethacin. Residual LRO in ground γ indomethacin shows memory of the γ crystalline form.

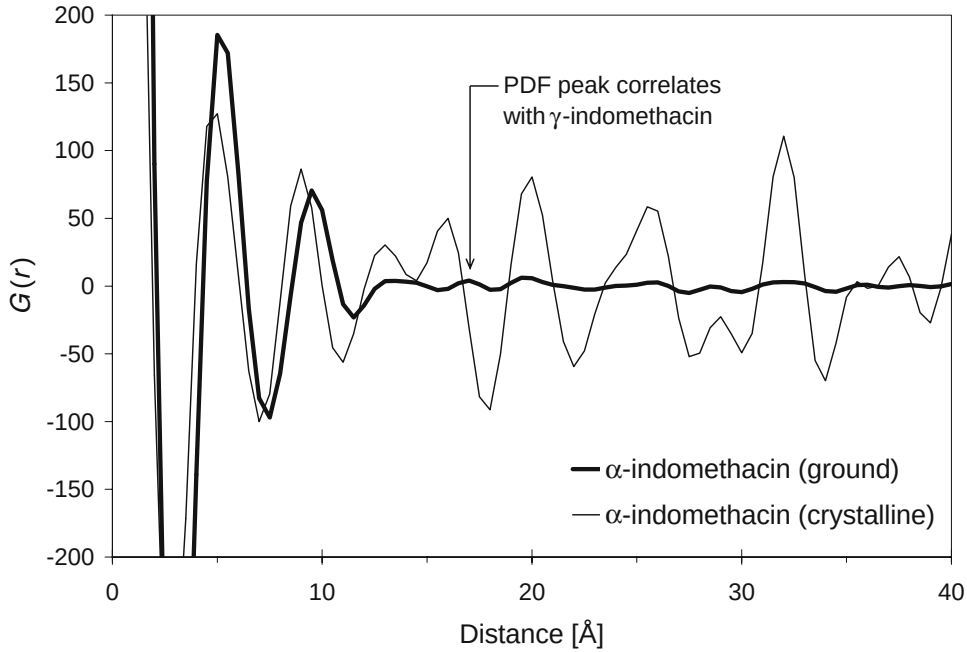

Fig. 13. PDF of cryoground α indomethacin and crystalline α indomethacin. Residual long-range order in cryoground α indomethacin shows memory of the α crystalline form and additional structure correlated to the γ crystalline form.

Form I shows no continuous peak broadening on the way to an amorphous state, behaving like the indomethacin polymorphs discussed above. However, the XRPD pattern of Form II shows the formation of an intermediate disordered nanocrystalline/glassy phase before collapsing to an amorphous phase.

The XRPD patterns obtained by grinding piroxicam Forms I and II for 60 min resulted in amorphous materials for both forms. The patterns for these samples show the same amorphous character but different residual LRO (12). The recrystallization behavior of the two amorphous materials was reported to be different. The amorphous material obtained from Form I recrystallized to Form I and exhibited a crystallization onset of 48°C. The PDF of amorphous Form I showed that the LRO of crystalline Form I was retained in the amorphous material and provided an easy pathway to recrystallization, resulting in a material that was not physically stable. In contrast, the PDF of the amorphous material obtained from Form II showed no correlation with the PDF of crystalline Form II and only a weak correlation was found with the PDF of crystalline Form I. This is proposed to be due to the more second order-like Type II disorder-disorder phase transition in the system that resulted in the loss of "memory" of LRO crystalline Form II. This material exhibited a recrystallization onset of 63°C. Upon recrystallization, a new Form III material was reported. The loss of memory not only thwarted conversion to Form I or II upon crystallization, but provided a new pathway to produce material described as Form III. This new pathway resulted in material that was more stable to recrystallization based on the recrystallization onset temperature. This example illustrates the need to use more than one technique to fully understand the type of X-ray amorphous materials (disordered nanocrystalline, glassy, or amorphous) as well as their related stabilities.

CONCLUSIONS

As the above examples illustrate, obtaining a material that exhibits an amorphous halo can represent any number of "X-ray amorphous" or disordered phases, ranging from disordered nanocrystalline to glassy or amorphous. Even amorphous materials can differ based on the extent of the microstructure and any residual LRO (seeds) present in the sample. This is not polyamorphism (53–55), but rather kinetically different disordered materials.

Since amorphous materials are metastable compared to crystalline pharmaceuticals, physical stability is an important parameter when investigating and possibly developing amorphous drug substances. Materials ground to or exhibiting the same X-ray amorphous pattern may crystallize at different times or to different crystalline forms. This can be perceived as a lack of control, resulting in amorphous materials that are not consistent. A better understanding of the short-range and long-range interactions in amorphous materials using PDFs and other data analysis techniques presented in this paper can help explain and possibly help control the physical stability of the materials. Data analysis of X-ray amorphous patterns play a significant role in addressing the primary regulatory concerns for commercialization: understanding, stability, and reproducibility.

All of the forms discussed here can be viable candidates for product development. FDA has acknowledged this in open forum and this is largely a result of the increase in understanding of amorphous materials in recent years. The key to producing a dosage form with the desired quality as well as gaining efficient regulatory acceptance is to understand as fully as possible the solid state being filed. Without sufficient demonstrated understanding one is essentially using an uncharacterized form with all of the associated risks.

The data generated within this study represent the initial modeling results for X-ray amorphous organic molecular materials. Further studies are required before general relationships between the crystalline, glassy, and amorphous forms of organic molecular systems can be firmly established.

ACKNOWLEDGMENTS

The authors would like to thank Paul Shields for collecting the XRPD data on microcrystalline cellulose and Igor Ivaniesevic for computational assistance. We would also like to thank Agam Sheth and the late David Grant for the use of the ground piroxicam data. This paper is dedicated to the memory of Professor David J. W. Grant who significantly contributed to our knowledge of solid-state pharmaceutics.

REFERENCES

1. B. C. Hancock and G. Zografi. Characteristics and significance of amorphous solids in pharmaceutical systems. *J. Pharm. Sci.* **86**:1–12 (1997).
2. P. G. Debenedetti. *Metastable Liquids : Concepts and Principles*, Princeton University Press, Princeton, New Jersey, 1996.
3. S. J. L. Billinge and M. F. Thorpe. *Local Structure from Diffraction*, Plenum, New York, 1998.
4. W. H. Zachariasen. The atomic arrangement in glass. *J. Am. Chem. Soc.* **54**:3841–3851 (1932).
5. B. Wunderlich. A classification of molecules, phases, and transitions as recognized by thermal analysis. *Thermochim. Acta* **340–341**:37–52 (1999).
6. C. B. Murray, D. J. Norris, and M. G. Bawendi. Characterization of nearly monodisperse CdE (E = sulfur, selenium, tellurium) semiconductor nanocrystallites. *J. Am. Chem. Soc.* **115**:8706–8715 (1993).
7. D. A. Keen and M. T. Dove. Total scattering studies of silica polymorphs: similarities in glass and disordered crystalline local structures. *Minerological Magazine* **64**(3):447–455 (2000).
8. S. R. Elliott. *Physics of Amorphous Materials,* 2 ed. Longman, London, 1990.
9. M. P. Fontana, R. Burioni, and D. Cassi. Generalized Landau Peierls instability: a novel perspective on the nature of glasses? *Philos. Mag. B.* **84**(13–16):1307–1311 (2004).
10 D. Kivelson, S. A. Kivelson, X. Zhao, Z. Nussinov, and G. Tarjus. A thermodynamic theory of supercooled liquids. **219**: 27–38 (1995). H. Tanaka. Two-order-parameter description of liqiuds. I. A general model of glass transition covering its strong to fragile limit. **111**(7):3163–3174 (1999). H. Tanaka. Two-order-parameter description of liqiuds. II. Criteria for vitrification and predictions of our model. **111**(7):3175–3182 (1999).
11. K. J. Crowley and G. Zografi. Cryogenic grinding of indomethacin polymorphs and solvates: assessment of amorphous phase formation and amorphous phase stability. *J. Pharm. Sci.* **91**:492–507 (2002).
12. (a) A. R. Sheth, S. Bates, F. X. Muller, and D. J. Grant. Local structure in amorphous phases of piroxicam from powder X-ray diffractometry. *Cryst. Growth Des.* **5**(2):571–578 (2005). (b) A. R. Sheth, S. Bates, F. X. Muller, and D. J. Grant. Polymorphism in Piroxicam. *Cryst. Growth Des.* **4**(6):1091–1098 (2004).
13. P. Debye. *Ann. d. Physik.* **46**:809–823 (1915).
14. T. Proffen. Analysis of occupational and displacive disorder using atomic pair distribution function: a systematic investigation. *Z. Kristallogr.* **215**:1–8 (2000).
15. T. Proffen, S. J. L. Billinge, T. Egami, and D. Louca. Structural analysis of complex materials using the atomic pair distribution function—a practical guide. *Z. Kristallogr.* **218**:132–143 (2003).
16. M. Bishop and C. Bruin. The pair correlation function: a probe of molecular order. *Am. J. Phys.* **52**:1106–1108 (1984).
17. A. Guinier. *X-ray Diffraction in Crystals, Imperfect Crystals, and Amorphous Bodies*, Dover, New York, 1994.
18. H. P. Klug and L. E. Alexander. *X-ray Diffraction Procedures for Polycrystalline and Amorphous Material*, Wiley, New York, 1974.
19. B. E. Warren. *X-ray Diffraction*, Dover, New York, 1990.
20. B. H. Toby and T. Egami. Accuracy of pair distribution function analysis applied to crystalline and non-crystalline materials. *Acta Crystallogr.* **A48**:336–346 (1992).
21. P. F. Peterson, E. S. Bozin, T. Proffen, and S. J. L. Billinge. Improved measures of quality for the atomic pair distribution function. *J. Appl. Crystallogr.* **36**:53–64 (2003).
22. V. Petkov, S. J. L. Billinge, S. D. Shastri, and B. Himmel. High-resolution atomic distribution functions of disordered materials by high-energy X-ray diffraction. *J. Non-Cryst. Solids* **293–295**: 726–730 (2001).
23. H. M. Rietveld. Line profiles of neutron powder-diffraction peaks for structure refinement. *Acta Crystallogr.* **22**:151–152 (1967).
24. H. M. Rietveld. A profile refinement method for nuclear and magnetic structures. *J. Appl. Crystallogr.* **2**:65–71 (1969).
25. M. Ferrari and L. Lutterotti. Method for the simultaneous determination of anisotropic residual stresses and texture by X-ray diffraction. *J. Appl. Phys.* **76**(11):7246–7255 (1994).
26. S. Matthies, L. Lutterotti, and H.-R. Wenk. Advances in texture analysis from diffraction spectra. *J. Appl. Crystallogr.* **30**:31–42 (1997).
27. L. Lutterotti, S. Matthies, and H.-R. Wenk. MAUD (Material Analysis Using Diffraction): a user friendly {Java} program for {Rietveld} Texture Analysis and more. *Proceeding of the Twelfth International Conference on Textures of Materials (ICOTOM-12)***1**:1599–1604 (1999).
28. R. C. Reynolds Jr. Diffraction by small and disordered crystals. Chapter 6. In D. L. Bish and J. E. Post (eds.), *Modern Powder Diffraction*, Mineralogical Society of America, Washington, DC, 1989.
29. J. M. Cowley. *Diffraction Physics*, North-Holland, Amsterdam, 1995.
30. S. Bates and I. Ivanisevic, manuscript in preparation.
31. S. R. Williams and A. P. Philipse. Random packing of spheres and spherocylinders simulated by mechanical contraction. *Phys. Rev. E.* **67**:051301 (2003).
32. W. Man *et al.*, Experiments on random packing of ellipsoids. *Phys. Rev. Lett.* **94**:198001 (2005).
33. A. Donev, J. Burton, F. H. Stillinger, and S. Torquato. Tetratic order in phase behavior of hard-rectangle system. *Phys. Rev. B.* **73**:054109 (2006).
34. R. W. James. The optical principles of the diffraction of X-rays. Chapter IX, *In The Scattering of X-rays by Gases, Liquids and Amorphous Solids*, Ox Bow, Woodbridge, 1962.
35. J. Perlstein. Molecular self-assemblies. 2. A computational method for the prediction of the structure of one dimensional screw, glide, and inversion molecular aggregates and implications for the packing of molecules in monolayers and crystals. *J. Am. Chem. Soc.* **116**:455–470 (1994).
36. Y. Nishiyama, J. Sugiyama, H. Chanzy, and P. Langan. Crystal structure and hydrogen bonding system in cellulose Iβ from synchrotron and neutron fiber diffraction. *J. Am. Chem. Soc.* **124**:9074–9082 (2002).
37. Y. Nishiyama, J. Sugiyama, H. Chanzy, and P. Langan. Crystal structure and hydrogen bonding system in cellulose Iα from synchrotron and neutron fiber diffraction. *J. Am. Chem. Soc.* **125**:14300–14306 (2003).
38. H. Batzer and Kreibich. Influence of water on thermal transitions in natural polymers and synthetic polyamides. *Polym. Bull.* **5**:585 (1981).
39. L. Salmen and E. Back. Moisture-dependent thermal softening of paper evaluated by its elastic modulus. *Tappi.* **63**:117–120 (1980).
40. J. A. Kaduk and P. Langan. Crystal structures and hydrogen bonding in celluloses Iα, Iβ, and II. Advances in X-Ray Analysis, Vol. 47. [Proceedings of the 52nd Annual Denver Conference on Applications of X-Ray Analysis, Held August 4–8, 2003, University of Denver, Colo.]. (2003).
41. P. Langan, S. Narayanasami, Y. Nishiyama, and H. Chanzy. Synchrotron X-ray structures of cellulose Iβ and regenerated cellulose II at ambient temperature and 100 K. *Cellulose* **12**(6):551–562 (2005).

42. G. Zografi, M. J. Kontny, A. Y. S. Yang, and G. S. Brenner. Surface area and water vapor sorption of microcrystalline cellulose. *Int. J. Pharm.* **18**:99–116 (1984).
43. P. J. Cox and P. L. Manson. γ-Indomethacin at 120 K. *Acta Crystallogr.* **E59**:o986–o988 (2003).
44. L. S. Taylor and G. Zografi. Spectroscopic characterization of interactions between PVP and indomethacin in amorphous molecular dispersions. *Pharm. Res.* **14**:1691–1698 (1997).
45. K. S. Masuda, S. Tabata, Y. Sakata, T. Hayase, E. Yomemochi, and K. Terada. Comparison of molecular mobility in the glassy state between amorphous indomethacin and slaicin based on spin-lattice relaxation times. *Pharm. Res.* **22**:797–805 (2005).
46. A. R. Sheth, J. W. Lubach, E. J. Munson, F. X. Muller, and D. J. W. Grant. Machanochroism of piroxicam accompanied by intermolecular proton transfer probed by spectroscopic methods and solid-phase changes. *J. Amer. Chem. Soc.***127**:6641–6651.
47. A. Salecki-Gerhardt and G. Zografi. Assessment of disorder in crystalline solids. *Int. J. Pharm.* **101**:237–247 (1994).
48. A. P. Simonelli, S. C. Mehta, and W. I. Higuchi. Dissolution rates of high energy sulfathiazole–povidone coprecipitates II: characteristics of form of drug controlling its dissolution rate via solubility studies. *J. Pharm. Sci.* **65**:355–361 (1976).
49. K. Crowley and G. Zografi. The effect of low concentrations of molecularly dispersed poly(vinylpyrrolidone) dispersions on indomethacin crystallization from the amorphous state. *Pharm. Res.* **20**:1417–1422 (2003).
50. V. Andronis and G. Zografi. Crystal nucleation and growth of indomethacin from the amorphous state. *J. Non-Cryst. Solids* **271**:236–248 (2000).
51. M. Yoshioka, B. C. Hancock, and G. Zografi. Crystallization of indomethacin from the amorphous state below and above its glass transition temperature. *J. Pharm. Sci.* **83**:1700–1704 (1994).
52. M. Otsuka and N. Kaneniwa. A kinetic study of the crystallization process of noncrystalline indomethacin under isothermal conditions. *Chem. Pharm. Bull.* **36**:4026–4032 (1988).
53. A. Ha, I. Cohen, X. Zhao, M. Lee, and D. Kivelson. Supercooled liquids and polyamorphism. *J.Phys. Chem.* **100**:1–4 (1996).
54. P. F. McMillan. Polymorphic transformations in liquids and glasses. *J. Mater. Chem.* **14**:1506–1512 (2004).
55. E. Y. Shalaev and G. Zografi. The concept of structure in amorphous states from the perspective of the pharmaceutical sciences. In H. Levine (ed.), *Progress in Amorphous Food and Pharmaceutical Systems*, The Royal Chemistry Society, London, 2002, pp. 11–30.